A superelastic alloy microgripper with embedded electromagnetic actuators and piezoelectric force sensors: a numerical and experimental study

2005 Smart Mater. Struct. 14 1265

(http://iopscience.iop.org/0964-1726/14/6/019)

INSTITUTE OF PHYSICS PUBLISHING SMART MATERIALS AND STRUCTURES
Smart Mater. Struct. **14** (2005) 1265–1272 doi:10.1088/0964-1726/14/6/019

A superelastic alloy microgripper with embedded electromagnetic actuators and piezoelectric force sensors: a numerical and experimental study

Deok-Ho Kim[1,5], Moon Gu Lee[2], Byungkyu Kim[3,6] and Yu Sun[4]

[1] Microsystem Research Center, Korea Institute of Science and Technology, PO Box 131, Cheongryang, Seoul, 130-650, Korea
[2] Mechatronics Center, Samsung Electronics, 416 Maetan-3dong, Paldal-gu, Suwon, Kyonggi-do, 443-742, Korea
[3] School of Aerospace and Mechanical Engineering, Hankuk Aviation University, Kyonggi-do 412-791, Korea
[4] Department of Mechanical and Industrial Engineering, University of Toronto, 5 King's College Road, M5S 3G8, Canada

E-mail: bkim@kist.re.kr

Received 14 October 2004, in final form 11 July 2005
Published 11 October 2005
Online at stacks.iop.org/SMS/14/1265

Abstract
This paper presents the analysis, design, and characterization of a superelastic alloy (NiTi) microgripper with integrated electromagnetic actuators and piezoelectric force sensors. The microgripper, fabricated by electro-discharge machining, features force sensing capability, large force output, and large displacements to accommodate objects of various sizes. The design parameters for the embedded electromagnetic actuators were selected on the basis of finite element sensitivity analysis. In order to make the microgripper capable of resolving gripping forces, piezoelectric force sensors were fabricated and integrated into the microgripper. The performance of the microgripper, the integrated force sensors, and the electromagnetic actuators was experimentally evaluated. A satisfactory match between experimental results and finite element simulations was obtained. Furthermore, comparison studies demonstrated that the superelastic alloy (NiTi) microgripper was capable of producing larger displacement than a stainless steel microgripper. Finally, experimental results of optical fiber alignment and the manipulation of tiny biological tissues with the superelastic microgripper were presented.

(Some figures in this article are in colour only in the electronic version)

1. Introduction

The need for microgrippers with high precision and reliable operation has recently increased for such applications as assembling and testing microsystem components and/or measuring mechanical properties of biological cells and tissues [1–5]. In emerging information technology (IT) and related industrial applications, there are many commercial microsystems in the mesoscale range that covers 100 μm–1 mm, requiring flexible precision assembly: for instance, hard drive read/write head assemblies, fiber optic assemblies, and RF switches/filters. Despite the importance and necessity of these applications, systematic approaches to practical

[5] Present address: Department of Biomedical Engineering, Johns Hopkins University, Baltimore, MD 21218, USA.
[6] Author to whom any correspondence should be addressed.

Table 1. Specifications of microgrippers made of different materials.

Material	Actuation principle	Arm length (μm)	Gripping stroke (μm)	Max. gripping force (mN)	Reference
Poly-Si	Electrostatic	500	9	—	[6]
TiNi	Shape memory alloy	1000	180	17	[12]
SU-8	Electro-thermal	650	15	—	[13]
	Piezoelectric	2000	170	—	[14]
Titanium	Piezoelectric	6000	1000	20	[4]
ICPF	Electroactive polymer	1200	—	—	[10]
Al/Cr	Pneumatic	1000	300	—	[15]

microgripper designs that integrate both actuators and sensors have not been adequately addressed. In this paper, we focus on the design of a microgripper for mesoscale applications.

Fundamental requirements of a microgripper for micromanipulation tasks include a large actuation-force-over-actuator-volume ratio, high actuation precision, and capabilities of sensing gripping forces. Due to recent advances in micromachining technology such as silicon surface/bulk micromachining [6, 7], laser micromachining [8], and electro-discharge machining (EDM) [2], several smart materials such as piezoelectric materials [9], electroactive polymers [10, 11], and shape memory alloys (SMAs) [12] have been used in the development of microgrippers. For example, silicon-based microgrippers using comb drive actuators [6] and electro-thermal actuators [7] have been introduced in microassembly applications. Nafion-based ionic conducting polymer films (ICPF) was used for developing two-finger actuators for aqueous sensing and manipulation [10]. An SMA microgripper machined by laser cutting was also reported, which provided a low-cost and compact solution for microrobotic manipulation tasks [12].

An overview of microgrippers reported in the literature is summarized in table 1. The gripping arm length of microgripper structures seems to be closely dependent on the chosen actuation principle and material. Despite the advantages of compactness and compatibility with MEMS (microelectromechanical systems) fabrication processes, electrostatically and electrothermally actuated microgrippers generate lower gripping forces compared to piezoelectric actuators and voice coil motors (VCMs). Besides generating lower gripping forces, gripping strokes of electrostatic and electrothermal microgrippers are typically limited to a few tens of microns, limiting their use in applications that require large displacements.

Although piezoelectric-actuator-based microgrippers have large actuation forces, they are limited in actuation strokes [16, 17]. Thus, they often require displacement amplifying mechanisms [17–19] that unfortunately reduce actuation forces. The second limitation of piezoelectrically driven microgrippers is that complex high-voltage amplifiers are required. The third limitation is the inherent hysteresis and creep, making the control of a piezoelectrically actuated microgripper difficult. Most piezoelectrically driven microgrippers previously developed were operated in open loop; thus, the precision and reliability cannot be guaranteed.

In our microgripper design, VCMs were employed as actuators. Despite the difficulty of miniaturizing VCM actuators compared to electrostatic or electrothermal actuators, there are several desired features of VCM actuators for microgripper design. Firstly, gripping strokes can be up to several hundreds of microns. Secondly, the linearity of VCM actuators is satisfactory and the linearization can be more straightforward than piezoelectric actuators, making the robust control of microgrippers possible. Thirdly, the required electronic circuit is simple and cost effective.

The NiTi superelastic alloy was used for the construction of the microgripper. From the perspective of material selection, the superelastic material has the ability to sustain large recoverable strain and to resist extreme stress without the occurrence of plastic deformations, which provides mechanical robustness and large gripping displacements [20]. The superelastic alloy with flexure hinge mechanism was used to enlarge the displacement of the microgripper arms. Design optimization was performed to obtain high actuation forces. Gripping force sensing was realized by integrating a piezoelectric polymer sensing element on the microgripper to detect deformations caused by gripping forces. Thus, the system is robust to external disturbances.

The paper is organized as follows. In section 2, the configuration of the microgripper design is described. In section 3, design of superelastic flexures, VCMs and piezoelectric polymer sensors using the finite element method is presented. The fabrication process of the microgripper and comparisons of the NiTi microgripper and a stainless steel microgripper are also described. In section 4, comparisons of the designed VCM actuators are made between experimental results and finite element simulations. Experimental performance and actuation properties of the superelastic materials are presented. Finally, conclusions are given in section 5.

2. System configurations

Figure 1 shows the schematic diagram of the microgripper design. The symmetrical structure consists of superelastic NiTi alloy gripping arms with the compliant hinge mechanism, VCM actuators, and force sensors as shown in figure 1(a). We employed the superelastic NiTi alloy as the structural material for the elastic flexure hinge mechanism to mechanically amplify microgripper displacements. Due to the superelastic property, the microgripper exhibits the ability to sustain large recoverable strain and to resist extreme stress without the occurrence of plastic deformations.

A voice coil motor (VCM) was used as an actuator for the microgripper. VCM actuators are widely used to actuate precision linear stages and the head of data storage devices such as optical disk drives and hard disk drives [21–23]. The

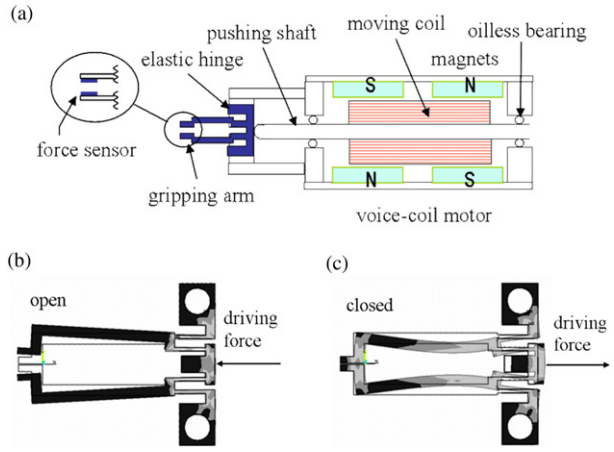

Figure 1. Configuration of the microgripper. (a) Schematics of the proposed microgripper design, (b) the actuation mode at the opening operation, and (c) the actuation mode at the closing operation.

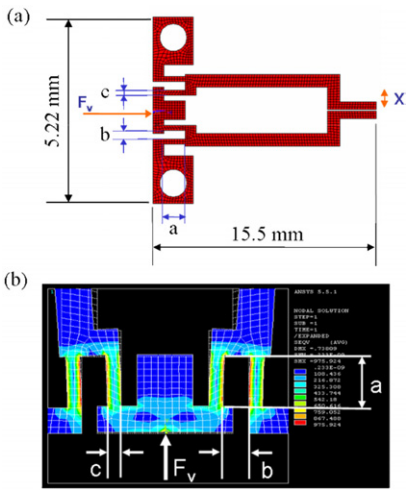

Figure 2. Finite element model of the proposed microgripper structure. (a) Overall view of meshed structure and (b) two-dimensional finite element model of the elastic flexure hinge defining three geometrical parameters and the actuation force to the microgripper structure.

actuator operates with Lorentz forces generated by a current-carrying conductor in a static magnetic field. The VCM generates linear forces proportional to applied currents. As shown in figure 1(a), the conductor (moving coil) is precisely aligned in between four rectangular neodymium iron boron magnets that provide a high gap field. Applying a voltage to the electromagnetic actuation element leads to linear motion of the pushing shaft. Consequently, the elastic flexure hinge in the gripper structure is deformed and the gripping arms are open (figure 1(b)). Reversing the applied voltage makes the gripping arms closed for grasping micro-objects (figure 1(c)).

Although force-controlled micromanipulation is desirable [24], most existing tweezer-type microgrippers are not capable of sensing gripping forces. In this design, piezoelectric PVDF polymer was used as a sensing material to provide gripping force feedback, which is required for handling fragile objects. Besides its excellent stability to chemicals, mechanical flexibility, and biocompatibility, the PVDF force sensor provides a high linearity, wide bandwidth, and high signal to noise (S/N) ratio [25, 26]. This unique combination of desired properties makes PVDF polymer a competitive candidate for force sensing elements. In order to electrically isolate the nickel electrodes of the PVDF force sensors, a thin parylene passivation layer was coated. Parylene is biocompatible, making the microgripper with PVDF force sensors suitable for manipulating biological cells and/or tiny tissues. Because the PVDF film is sandwiched between parylene coated layers, there is sufficient thermal insulation which reduces the pyroelectric effect of PVDF.

3. Design and fabrication

3.1. Design of superelastic flexures

The geometry of the microgripper (overall length 15.5 mm, overall width 5.22 mm, thickness 0.5 mm) is shown in figure 2(a). The core component of the gripper is the superelastic flexure hinge as shown in figure 2(b). Finite element simulation was conducted for analyzing the displacement and stress of the gripper with respect to the geometrical parameters in the flexure hinge design. The simulation objective was to find the pseudo-optimal design parameters, maximize the displacements at the gripper tip, and avoid the fatigue effects due to local stress concentration. In order to compare the material effect of superelastic NiTi alloy and stainless steel (SUS304), the material properties of the NiTi and SUS304 microgrippers were also considered in the simulation. In plane stress analysis, Young's modulus was assumed to be 198 GPa for SUS304 and 40 GPa for NiTi alloy and Poisson's ratio was 0.3 for SUS304 and 0.33 for NiTi alloy. Figure 3 shows the maximum displacement at the gripper tip with respect to variations in the design parameters under the assumption that 500 mN force (i.e. F_v shown in figure 2(b)) is constantly applied to the central point. Based on the simulation results, geometrical parameters $a = 1.6$ mm, $b = 0.65$ mm, $c = 0.35$ mm were chosen in the superelastic flexure design. Simulation results also indicated that the maximum displacement of the superelastic NiTi gripper is larger than that of the stainless microgripper. The maximum stress does not exceed a material-dependent critical limit, above which plastic deformation could occur.

The wire EDM method was used to fabricate the NiTi-alloy-based microgripping arms. The EDM method allows for constructing higher-aspect-ratio structures, such as 500 μm thick microgrippers, while the Nd YAG laser machining method was limited to machining structures up to 300 μm thick. The high aspect ratio of the microgripper structures is advantageous to avoid out-of-plane bending and achieve stable handling operation of high-aspect-ratio micro-objects with the enhanced surface contact area of gripping arms. For characterizing mechanical properties of materials, two microgrippers with the same design parameters were fabricated from the superelastic alloy (NiTi) and stainless steel (SUS304).

3.2. Design of VCM

We employed a VCM for actuating the microgripper and performed design optimization of the VCM using a finite

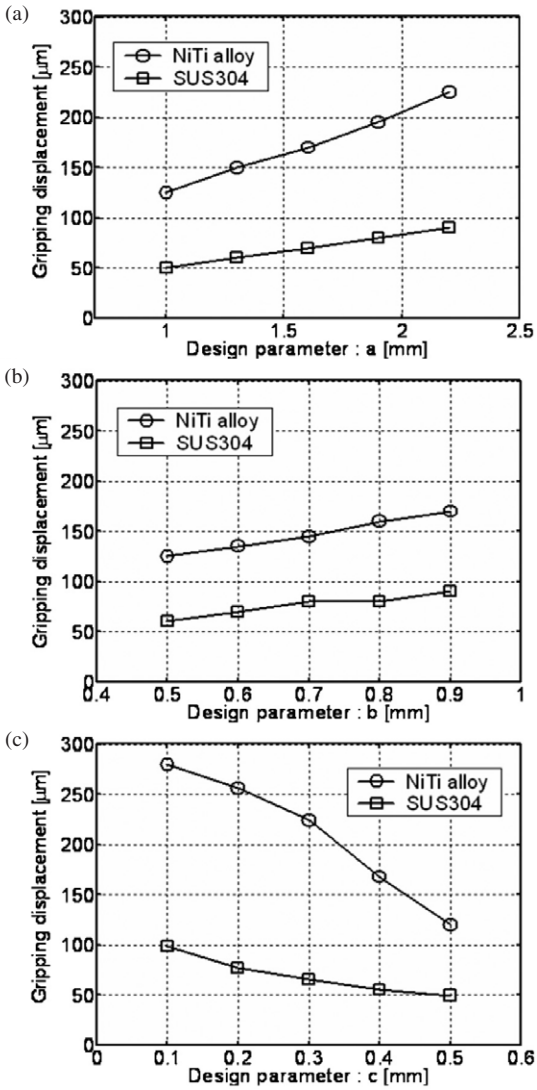

Figure 3. Sensitivity analysis: the maximum displacement changes with respect to different geometrical parameters in the elastic flexure hinge.

element method (FEM). The VCM consists of magnets (Korea Magnet Alloy Co., N-27, $H_c = 1.05$ kOe, $B_r = 1.05$ kG), coil windings (copper diameter $d = 0.150$ mm, enamel diameter $D = 0.177$ mm, 296 turns), and several jigs. The jigs include a bobbin on which the coil is wound and a backing plate to which magnets are attached. The actuating force is delivered to the microgripper arms through the bobbin and backing plate.

The design parameters of the VCM are shown in figure 4(a). Through the establishment of a finite element model as shown in figure 4(b), the magnetic flux and flux density on the coil were calculated and the results are shown in figure 5. The magnetic flux density distribution shown in figure 5(b) is not exactly symmetrical because the magnetic field induced by the coil is superposed to the permanent magnetic field. The actuation force corresponding to the applied input voltage was calculated by integrating the Maxwell stress tensor.

The VCM is operated by a voltage-driven method. The voltage applied to the VCM is proportional to the current since the VCM is controlled in a quasi-static manner. The variation

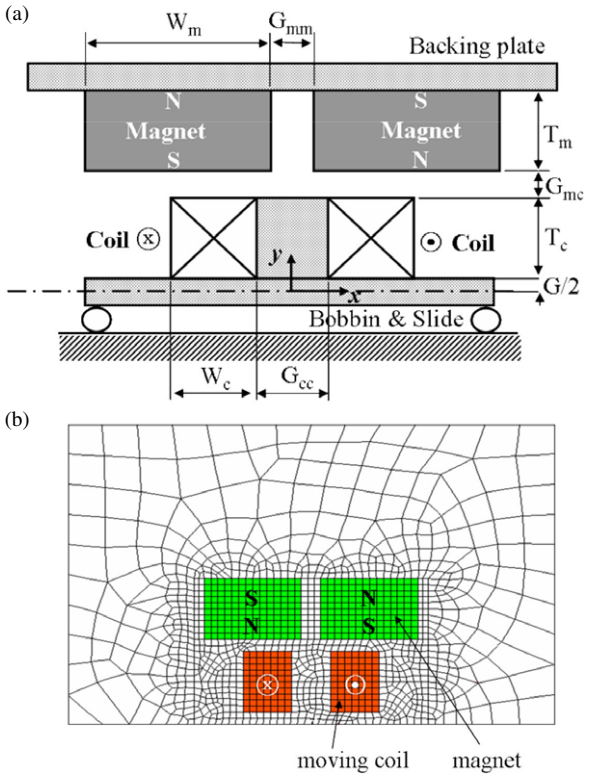

Figure 4. Voice coil motor for actuating the microgripper. (a) Cross sectional view and (b) two-dimensional finite element model (half model).

Table 2. Design parameters of the VCM.

Design parameters	Nomenclatures	Value (mm)
Width of coil winding block	W_c	2.5
Thickness of coil winding block	T_c	3.5
Width of magnet	W_m	5.0
Thickness of magnet	T_m	2.5
Gap between magnet and coil block	G_{mc}	0.75
Gap between two coil blocks	G_{cc}	2.0
Gap between two magnets	G_{mm}	1.0
Central air gap	G	1.5

of actuating forces with respect to the design parameters was investigated by fixing the input voltage at 5 V. Figure 6 shows the sensitivity analysis results of actuation force variations with respect to coil diameters and the number of turns from the finite element simulation. It needs to be noted that these design parameters are inextricably coupled to vary actuating forces. For example, when the cross-sectional area of a coil winding block is constant, a decrease of coil diameter causes an increase in the number of coil turns. More turns increase the coil's effective length, which further increases resistance, leading to a smaller current in the coil. Although a larger number of turns increase actuating forces, the corresponding decrease of current in the coil due to a larger number of turns reduces actuation forces. In order to optimize the design to achieve a high actuation force per unit volume (up to 77.6 mN mm^{-2} V^{-1}), finite element analysis with constraints of driving voltage and size for miniaturizing the VCM was conducted. The selected design parameters are listed in table 2.

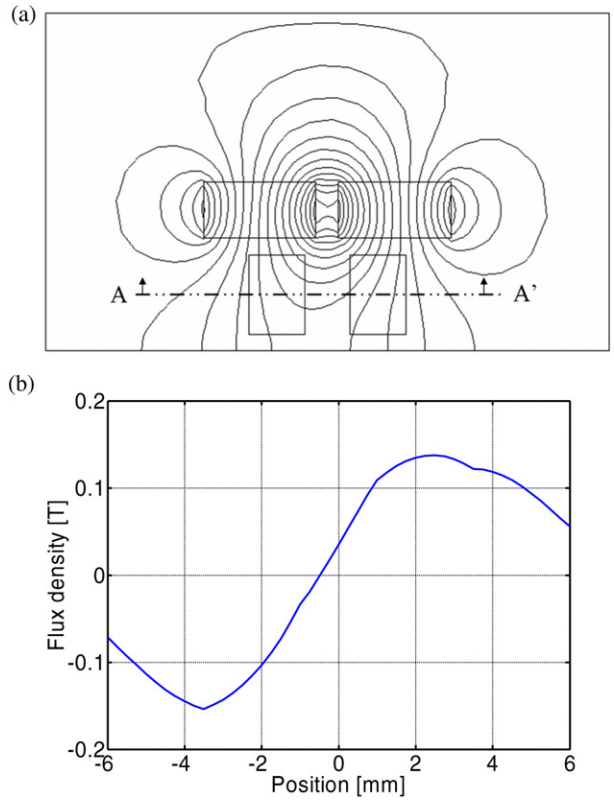

Figure 5. Magnetic field distribution on the coil of the VCM. (a) Magnetic flux line and (b) flux density along the line AA′ in (a).

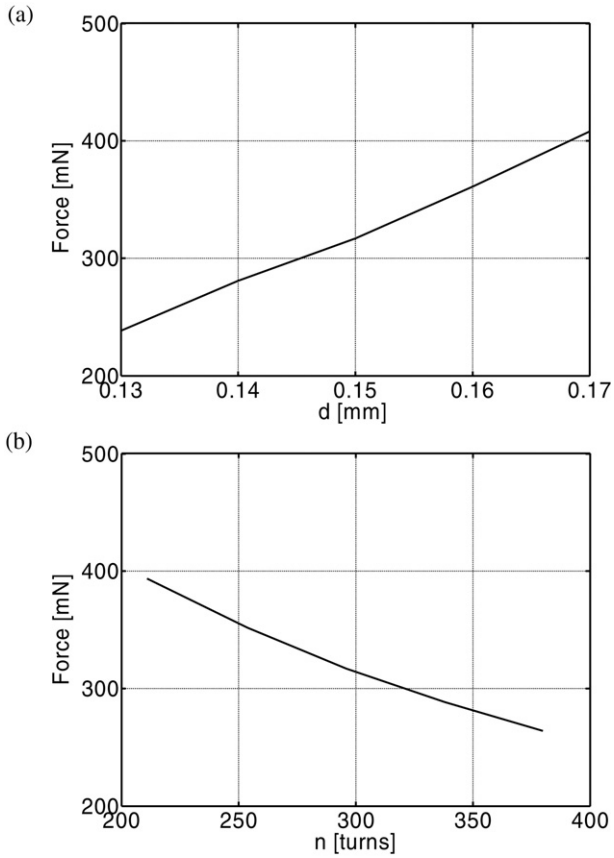

Figure 6. Sensitivity analysis: actuating force changes with respect to (a) the diameter of the coil and (b) the winding number of the coil.

3.3. Design of gripping force sensor

In order to resolve gripping forces, rectangular piezoelectric PVDF polymer layers (28 μm piezo film sheet from Measurement Specialties Inc.) were cut using a dicing saw. Figure 7 shows a schematic diagram of the miniaturized PVDF force sensor, where the two flat surfaces of the PVDF film are attached to nickel electrodes (thickness 2 μm) that provide electrical connections to an amplifier. The nickel electrodes on PVDF polymer film layers were bonded with gold wires using silver epoxy (model D-500, Dotite electroconductive silver paste) and cured for four hours at room temperature. As discussed in section 2, the PVDF force sensor was then sandwiched between parylene coated layers (thickness 6 μm) that provide sufficient thermal insulation to reduce the pyroelectric effect of PVDF.

In order to compare the experimental results to simulation results, the commercial finite-element code, CoventorWare, was used for the structural and piezoelectric coupled simulations. The finite element model was created for a flat layered force sensor. In order to reduce computation time, a quarter symmetric modeling technique was employed. For solving the governing differential equation, the FE model for the flat layered force sensor was meshed with brick elements and the contact mechanical load was applied to the surface of the force sensor. Structural–piezoelectric coupled analysis was performed on the 3D model with known material properties and symmetric boundary conditions to analyze the effect of mechanically applied stress on the behavior of the PVDF film sensor with parylene coating.

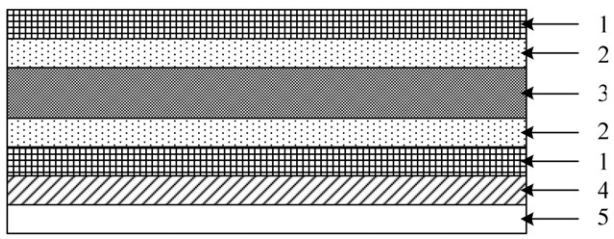

Figure 7. Layered structure of the PVDF force sensor. (1) Parylene layer (thickness 6 μm). (2) Nickel layer (thickness 2 μm). (3) PVDF film layer (thickness 28 μm). (4) Glue layer. (5) Microgripper arm (NiTi alloy).

4. Experiments

Prior to the integration into the complete microgripper system, VCM actuators and force sensors were experimentally characterized and compared to simulation results. The actuating forces of the VCM were measured using the experimental set-up shown in figure 8(a). The generated forces were transmitted to a rod that was attached to the end of the slider and then exerted on a load cell (model GSO-50, Transducer Techniques; full scale 500 mN, accuracy 0.25 mN). Figure 8(b) shows the measurement and finite element analysis results. The measured forces are larger than simulation results because the forces generated by the end turns of the coil

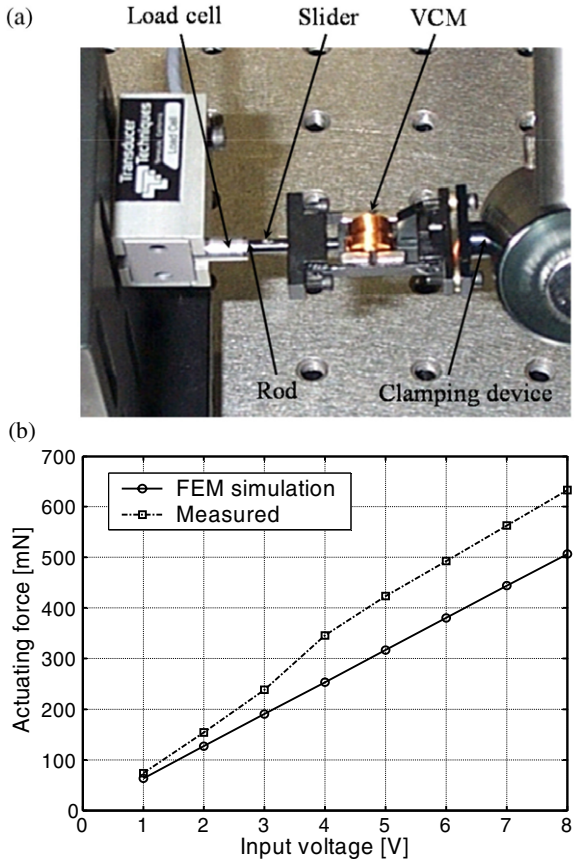

Figure 8. Characterization of the VCM performance. (a) Experimental set-up for measuring actuating forces of the VCM and (b) actuation forces of the VCM from experimental measurements and finite element analysis.

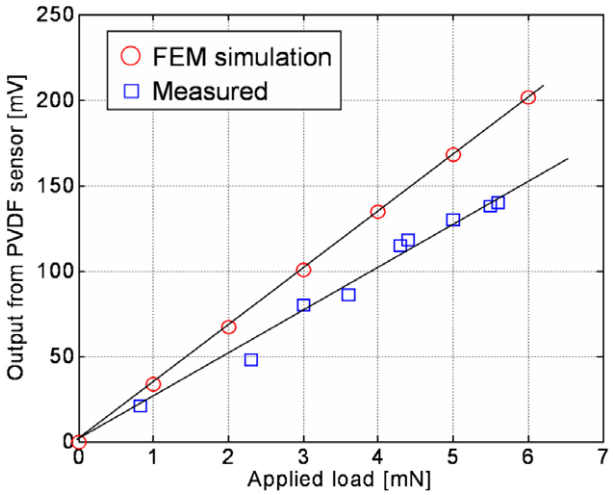

Figure 9. Comparison between simulated response of the PVDF force sensor and experimental measurement results.

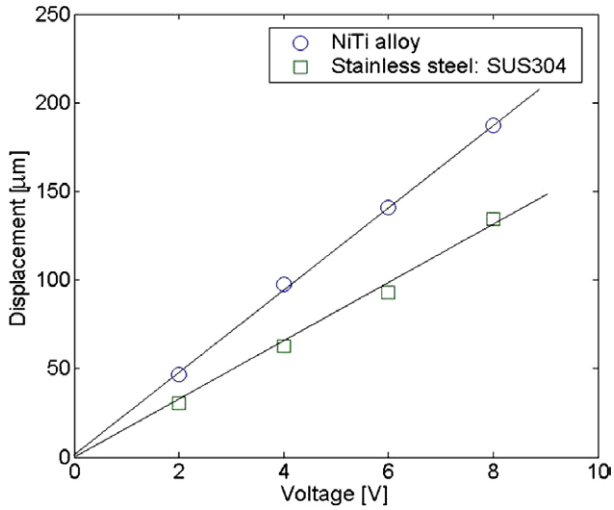

Figure 10. Experimental results of the gripping arm displacements of the NiTi alloy microgripper and the stainless steel (SUS304) microgripper. The actuation signal is a 1 Hz square wave.

appeared in measurements while the effect from the end turns of the coil is difficult to include in a two-dimensional finite element model. The measured actuating forces indicate that the optimally designed VCM actuator has linear characteristics and is capable of producing a maximum force of 630 mN at 8 V input voltage.

The PVDF force sensor (length 6 mm, width 2 mm, thickness 0.5 mm) was also experimentally tested. In a typical micro-grasping task, motion is generally slow (approximately from 0.1 to 10 Hz). Although PVDF sensors are usually for detecting dynamic deformations, signals in the low frequency range down to a few mHz can still be detected with proper circuit designs [27]. In our experiments, a commercial charge amplifier (model 5015B, Kistler) was used to effectively capture force signals in the low frequency range. The PVDF force sensor was glued onto a piezoelectric vibration unit (model PSI-5A4E, Piezo Systems). Forces were applied to the PVDF force sensor by the piezoelectric vibration unit with a 1 Hz sinusoidal signal to touch a 1 mm diameter circular probe attached to a commercial load cell. Figure 9 shows a comparison of sensor voltage outputs predicted by FEM analysis and the experimental measurement results. Based on the experimental measurements, the force sensor was determined to have a sensitivity of 39.5 mN V^{-1} and a linearity of $\pm 6.5\%$. The miniaturized PVDF force sensor was finally bonded on superelastic NiTi alloy gripping arms using non-conductive glue where the maximum strain occur during the gripping operation. Fine movements needed for precise manual bonding were produced by a 3-DOF micromanipulator (model MP-285, Sutter) with a travel of 22 mm and a resolution of 0.04 μm in each axis. The overall specifications of the microgripper are summarized in table 3. The initial gap between the two gripping arms is 100 μm, adjustable according to the size and shape of objects to be manipulated. The maximum size of objects that the gripper can grip is 400 μm. The adjustable initial gap between microgripper arms makes the microgripper capable of manipulating objects of various sizes.

The performance of the superelastic alloy microgripper was characterized and compared to that of a stainless steel microgripper. These two microgrippers have the same geometrical specifications and were tested with the same VCM unit. Finally displacement and force characterizations were performed on the gripper itself. Figure 10 shows the gripping arm displacements with respect to voltages applied to the

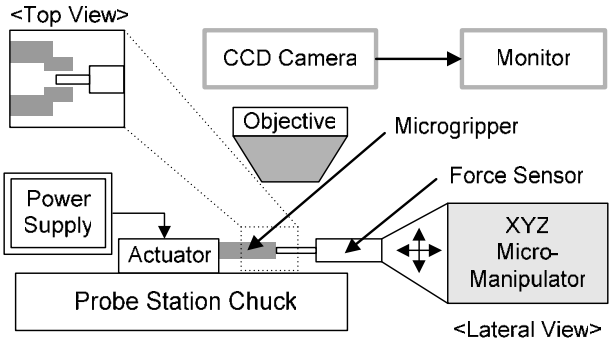

Figure 11. Schematic drawing of the experimental set-up of characterizing the exerted force at the gripper tip.

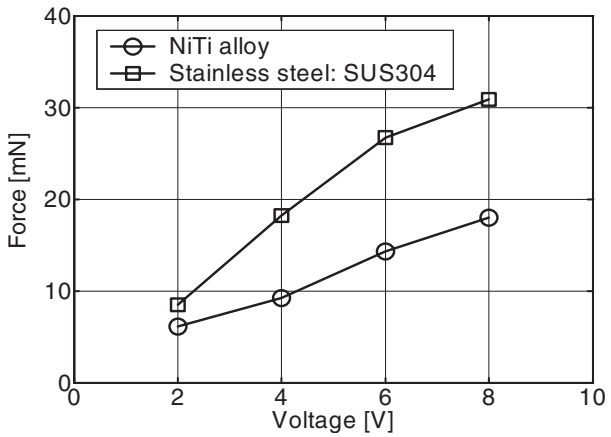

Figure 12. Experimental results of the exerted force at the tip of the superelastic alloy microgripper and the stainless steel microgripper.

VCM, measured with a laser displacement sensor (model LK 3100, Keyence; full scale 1 mm, accuracy 0.5 μm). The results shown in figure 10 are open-loop step responses of the micrograsping arms' position actuated by a 1 Hz square wave. The superelastic alloy microgripper is capable of producing larger gripper strokes/displacements than the stainless microgripper. Figure 11 shows a schematic diagram of the experimental set-up for characterizing gripping forces. A piezoresistive force sensor (model AE 801, Sensorone) was used to measure the exerted force at the gripper tip. The piezoresistive force sensor was located between the gripping arms. Initially, the gripping arms were in contact with the surface of the piezoelectric cantilever force sensor. When the reversing voltage was applied to the VCM actuator, the gripping arms started to close and apply forces to the piezoresistive force sensor. The output of the gripping force response of the superelastic alloy gripper along with the output of the stainless steel gripper is shown in figure 12. The actuation signal applied to VCM was a 1 Hz sinusoidal wave. As shown in figure 12, the measured gripping forces increase with higher applied voltages. The maximum gripping force measured was 18 mN for the superelastic alloy gripper and 30.9 mN for the stainless steel gripper. The lower, but sufficient gripping forces produced by the superelastic alloy microgripper were due to the flexible NiTi structure, which are desired for manipulating fragile micro-objects and

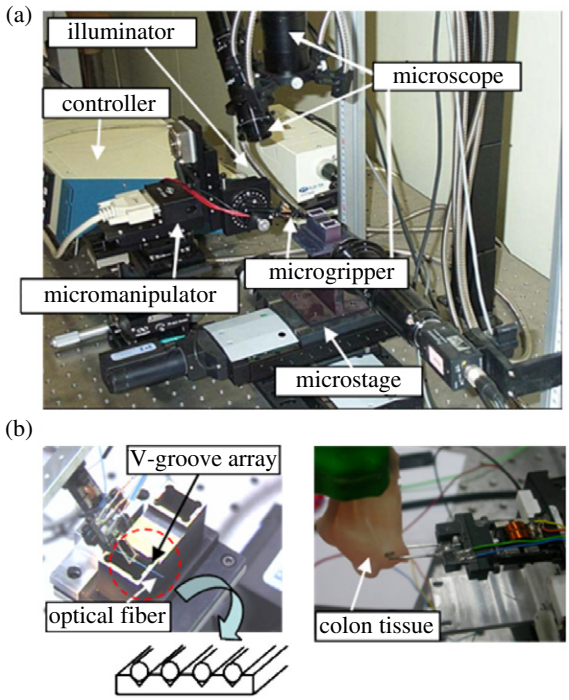

Figure 13. Applications of the integrated microgripper in a micromanipulation system. (a) The micromanipulation system set-up integrated with the superelastic microgripper, (b) optical fiber alignment, and (c) the manipulation of tissue in the colon with the adherent mucus removed *in vitro*.

Table 3. Specifications of the superelastic alloy microgripper.

Item	Specification
Actuator	Linear voice coil motor
Max. pushing force	600 mN
Max. gripping force	18 mN
Stroke of gripping	300 μm
Sensor	Polyvinylidene fluoride (PVDF) polymer
Resolution of force sensing	39.5 mN V^{-1}
Linearity	$\pm$6.5%
Weight	19.1 g (total), 0.12 g (gripper hands)
Dimension (gripper hands)	85 mm $\times$ 8 mm $\times$ 22 mm (total) 15.5 mm $\times$ 5.22 mm $\times$ 0.5 mm

producing large displacements. The gripping forces up to 20 mN produced by the superelastic microgripper would be suitable for applications such as optical fiber alignment [28], the assembly of a watch gear [29] and the manipulation of biological samples [30].

As shown in figure 13(a), a micromanipulation system integrated with the superelastic microgripper was constructed to perform fine alignment of optical fibers (diameter 125 μm) and to manipulate tiny biological tissues (tissue in the colon with the adherent mucus removed; thickness 116 μm). The system consisted of the integrated superelastic microgripper, an x–y microstage (model M-037 DG, PI), a 3-DOF micromanipulator (model MP-285, Sutter), lateral and vertical microscopes, and a haptic device (model PHANToM 1.5 Premium, SensAble Technologies) for force feedback based

micromanipulation. The integrated superelastic microgripper was successfully applied to damage-free alignment of optical fibers in an array format and the manipulation of tissues in the colon with the adherent mucus removed. Figures 13(b) and (c) are snapshots from the micromanipulation experiments. The maximum detected forces during the manipulation tasks were 5 mN for tissue handling and 13 mN for optical fiber alignment. In these micromanipulation tasks, microforce feedback was provided by the integrated superelastic microgripper via the haptic device to a human operator for secure grasping without applying too large a force to avoid damaging micro-objects.

5. Conclusions

This paper presents the development of a superelastic alloy microgripper with integrated electromagnetic actuators and piezoelectric force sensors. The microgripper was capable of producing large gripping strokes up to 300 μm and gripping forces up to 18 mN. Design simulation and optimization of the electromagnetic actuators and piezoelectric force sensor were conducted by finite element analysis. The piezoelectric force sensors provided a sensitivity of 39.5 mN V^{-1}. Comparisons were made between design simulations and experimental characterization results, and satisfactory agreements were obtained. Finally, this superelastic-alloy-based microgripper was successfully integrated in a micromanipulation system and applied to optical fiber alignment and the manipulation of tiny biological tissues.

Acknowledgments

This work was supported by the 21st Century's Frontier R&D Projects, under the contract number MS-02-324-01, sponsored by the Ministry of Science and Technology, Korea.

References

[1] Ansel Y, Schmitz F, Kunz S, Gruber H P and Popovic G 2002 Development of tools for handling and assembling microcomponents *J. Micromech. Microeng.* **12** 430–7
[2] Menciassi A, Scalari G, Eisinberg A, Anticoli C, Francabandiera P, Carrozza M C and Dario P 2001 An instrumented probe for mechanical characterization of soft tissues *Biomed. Microdev.* **3** 149–56
[3] Nelson B J, Zhou Y and Vikramaditya B 1998 Sensor-based microassembly of hybrid MEMS devices *IEEE Control Syst.* **18** 35–45
[4] Thornell G, Bexell M, Schweitz J and Johansson S 1996 Design and fabrication of a gripping tool for micromanipulation *Sensors Actuators* A **53** 428–33
[5] Yang G, Gaines J A and Nelson B J 2003 A supervisory wafer-level 3D microassembly system for hybrid MEMS fabrication *J. Intell. Robot. Syst.* **37** 43–68
[6] Kim C J, Pisano A P, Muller R S and Lim M G 1992 Polysilicon microgripper *Sensors Actuators* A **33** 221–7
[7] Du H, Su C, Lim M K and Jin W L 1999 A micromachined thermally-driven gripper: a numerical and experimental study *Smart Mater. Struct.* **8** 616–22
[8] Bordatchev E V and Nikumb S K 2003 Microgripper: design, finite element analysis and laser microfabrication *Proc. Int. Conf. on MEMS, Nano and Smart Syst.* pp 308–12
[9] Park J and Moon W 2003 A hybrid-type micro-gripper with an integrated force sensor *Microsyst. Technol.* **9** 511–9
[10] Zhou W and Li W J 2004 Micro ICPF actuators for aqueous sensing and manipulation *Sensors Actuators* A **114** 406–12
[11] Zhou W, Chan H Y, To K H, Lai W C and Li W J 2004 Polymer MEMS actuators for underwater micromanipulation *IEEE/ASME Trans. Mechatron.* **9** 334–42
[12] Kohl M, Just E, Pfleging W and Miyazaki S 2000 SMA microgripper with integrated antagonism *Sensors Actuators* **83** 208–13
[13] Chronis N and Lee L P 2005 Electrothermally activated SU-8 microgripper for single cell manipulation in solution *J. Microelectromech. Syst.* **14** 857–63
[14] Choi H S, Lee D C, Koo S S and Han C S 2005 The development of microgripper with a perturbation-based configuration design method *J. Micromech. Microeng.* **15** 1327–33
[15] Ok J, Chu M and Kim C J 1999 Pneumatically driven microcage for micro-objects in biological liquid *Proc. IEEE Int. Conf. Microelectromech. Syst.* (Piscataway, NJ: IEEE) pp 459–63
[16] Haddab Y, Chaillet N and Bourjault A 2000 A microgripper using smart piezoelectric actuators *Proc. IEEE/RSJ Int. Conf. Intell. Robots Syst.* pp 659–64
[17] Goldfarb M and Celanovic N 1999 A flexure-based gripper for small-scale manipulation *Robotica* **17** 181–8
[18] Krijnen G, Haanstra R, Potters F, Berenschot J W, Harrach S and Elwenspoek M 2003 Protruding microgripper with force amplification and parallel jaw motion for *in situ* sample manipulation in SEM and FIB-Machines *Proc. Int. Conf. on Solid-State Sensors, Actuators and Microsystems* pp 268–71
[19] Pokines B J and Garcia E 1998 A smart material microamplification mechanism fabricated using LIGA *Smart Mater. Struct.* **7** 105–12
[20] Zhao L C and Cai W 2000 Shape memory and superelastic materials and their applications in engineering and biomedical fields *Rare Metal Mater. Eng.* **29** 33–5
[21] Lee M G, Gweon D G and Kim S M 1997 Modelling and optimal design of a fine actuator for optical heads *Mechatronics* **7** 573–88
[22] Lee M G, Jeong J H and Gweon 2003 A comparative analysis of voice coil motors with multi-segmented and conventional magnet array for rotating data storage devices *Japan. J. Appl. Phys.* **42** 3394–5
[23] Lee M G, Lee S Q and Gweon D G 2004 Halbach magnet array and its application to linear motor *Mechatronics* **14** 115–28
[24] Molhave K and Hansen O 2005 Electro-thermally actuated microgrippers with integrated force-feedback *J. Micromech. Microeng.* **15** 1265–70
[25] Dargahi J, Parameswaran M and Payandeh S 2000 A micromachined piezoelectric tactile sensor for an endoscopic grasper-theory, fabrication and experiments *J. Microelectromech. Syst.* **9** 329–35
[26] Kim D H, Kim B and Kang H 2004 Development of a piezoelectric polymer-based sensorized microgripper for micromanipulation and microassembly *Microsyst. Technol.* **10** 275–80
[27] Benech P, Chamberod E and Monllor C 1996 Acceleration measurement using PVDF *IEEE Trans. Ultrason. Ferroelectr. Freq. Control* **43** 838–43
[28] Kim B, Kang H, Kim D H and Park J O 2005 A flexible microassembly system based on hybrid manipulation scheme for manufacturing photonics components *Int. J. Adv. Manuf. Technol.* at press
[29] Ferreira A, Agnus J, Chaillet N and Breguet J M 2004 A smart microrobot on a chip: design, identification, and control *IEEE/ASME Trans. Mechatron.* **9** 508–19
[30] Carrozza M C, Dario P, Menciassi A and Fenu 1998 A manipulating biological and mechanical micro-objects using LIGA-microfabricated end-effectors *Proc. IEEE Int. Conf. on Robotics Automation* (Piscataway, NJ: IEEE) pp 1811–6